Low-Frequency Noise Measurements for Electromigration Characterization in BEOL Interconnects

S. Beyne[1,2], K. Croes[2], O. Varela Pedreira[2], L. Arnoldi[2], M. H. van der Veen[2], I. De Wolf[1,2], and Zs. Tőkei[2]

[1]MTM, KU Leuven, Kasteelpark Arenberg 44 bus 2450, B-3001, Leuven, Belgium
[2]imec, Kapeldreef 75, B-3001, Leuven, Belgium

***Abstract*—In this paper we discuss a new EM test methodology, based on low-frequency noise (LFN) measurements. The main advantages of LFN over the standard accelerated EM tests are that they are non-destructive, much faster, closer to operation conditions and provide more fundamental understanding. Using the LFN technique, we study the EM properties in sub-30 nm line-width Cu interconnects with various metallization schemes. Furthermore, the EM activation energies of alternative metal interconnects (Ru, Co, W) are studied by means of LFN measurements.**

***Index Terms*—Electromigration, low-frequency noise, interconnects, BEOL reliability, ruthenium, cobalt**

I. Introduction

Electromigration (EM) is a mass transport resulting from the momentum exchange between the electrons accelerated by an electric field and the metal ions of a conductor. EM is a major problem for the reliability of electronic interconnects, as it may eventually lead to voids and therefore failure of electronic components.

Electromigration-induced mass transport proceeds along diffusion paths, each with a specific activation energy, E_A. In copper interconnects, the main diffusion paths to be considered are the Cu/dielectric interface, the copper surface and the grain boundaries. Potential measures to control them are barriers/liners, capping layers and doping, respectively. Nevertheless, testing the electromigration properties of different interconnect structures and metallization schemes, remains crucial to characterize their EM reliability. Standard electromigration tests are done by performing accelerated tests at highly elevated temperatures and current densities, followed by extrapolation of the failure times to normal operation conditions using Black's law [1]. This test procedure has some important drawbacks; it is still rather time-consuming (a test may take several weeks to even months), destructive, gives only limited physical understanding because the activation energy may be an average value of different diffusion mechanisms occurring in parallel, rather than stemming from one specific mechanism and finally the extrapolation to normal operation conditions, may not always be justified [2]. Therefore, a new EM test method, using non-destructive low-frequency noise measurements has been proposed [3–5]. In this paper, the test method will be explained and various applications will be shown. For a theoretical validation of the technique, the reader is referred to ref. [5]. Furthermore, the test method is applied to study the EM mechanisms in sub 30 nm half-pitch copper interconnects. A second problem addressed in this paper, is the study of electromigration in alternative metal interconnects. Copper is reaching its limits as interconnect material of choice because of its unacceptable resistivity increase [6, 7] and insufficient EM performance below 20 nm half-pitch [8, 9]. Therefore, a transition to alternative interconnect metals in the most narrow interconnect lines is incontrovertible. Potential candidates are cobalt and ruthenium. Studying their EM properties using the standard accelerated test method is particularly difficult in this case because they exhibit very long EM lifetimes [10]. As such, very high stress conditions have to be applied in order to observe failures within a reasonable time-frame. This could, however, lead to different failure mechanisms than under normal conditions, cause excessive Joule heating, or even alter the microstructure of the materials during the test, making life-time extrapolations even more questionable. In this paper we show that the EM activation energies in Ru and Co interconnects can be obtained using LFN measurements.

II. Low-frequency noise measurements

When a constant current, i_C is applied to an interconnect, the output current, $i(t)$, will be composed of that constant current plus random current fluctuations, $\Delta i(t)$, resulting from the interaction of electrons with the interconnects sidewalls, defects, phonons etc. These fluctuations can be analyzed in the frequency domain by means of a Fourier transformation. The power spectral density of the fluctuations can then be calculated using for example the Welch method [11]. This procedure is schematically shown in Fig. 1. The noise originating from current fluctuations in metals, typically exhibits a PSD proportional to $1/f^m$, with $0 < m < 2$ in the low-frequency range; we will refer to this noise as low-frequency noise (LFN). At larger frequencies, where thermal noise is dominant, the PSD is frequency independent and proportional to $4\mathrm{k_B T/R}$ (k_B is the Boltzmann constant, T the temperature and R the line resistance). The exact origins of LFN in metals remain largely unknown, but that does not limit its applications. Indeed, a specific LFN spectrum results from a certain stochastic process of electron scattering and thus

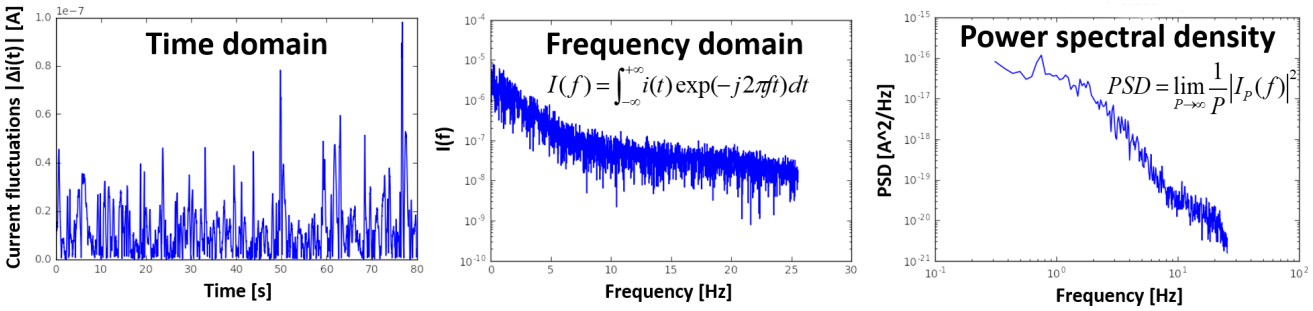

Fig. 1: When a constant current i_C is applied to an interconnect, random current fluctuations, $\Delta i(t)$, are detected on the output current $i(t)$ (left). The Fourier transform, $I_P(f)$, of $i(t)$ is calculated (center), which is used to calculate the PSD (right). P denotes the period of the periodic signal.

a change in LFN spectrum implies an underlying change in electron scattering mechanism. Therefore, LFN measurements can be used to study EM degradation, the impact of the conductor composition, pre-existing defect concentration, etc. The low-frequency noise measurements reported in this work, have been carried out using dedicated commercial equipment. Both the Proplus 9812B and Keysight's E4727A have been used. These systems are equipped with amplifiers, filters and appropriate shielding to limit the impact of noise caused by the surroundings. Schematics of the respective setups can be found in ref. [3, 4]. The measured frequency range was typically 1Hz to 100KHz. A thermal chuck was used to test samples in the temperature range $25 \rightarrow 200°$C.

III. A NOVEL ELECTROMIGRATION TEST METHOD

In this section, the application of low-frequency noise measurements to characterize electromigration is discussed. This work has previously been published in references [3, 4] and a summary of the main findings is provided here.

A. *Calculation of electromigration activation energies*

The temperature dependence of the low-frequency noise in metals can be used to calculate the activation energies of diffusion mechanisms. Experimentally, it is observed that at certain temperatures, the LFN PSD exhibits a maximum or peak. The temperature at which this peak occurs can be used to calculate the activation energy, by means of the phenomenological model of Dutta, Dimon, and Horn [12, 13]. This so-called 'DDH-model', is the most generally accepted and enables the calculation of activation energies.

1) Methodology: The DDH-model assumes that the low-frequency noise spectrum originates from a large number of fluctuations, which each have a Lorentzian spectrum

$$S(\omega) \propto \frac{\tau_c}{\omega^2 \tau_c^2 + 1}, \tag{1}$$

with characteristic time τ_C. The radial frequency is denoted by ω. Instead of assuming a constant τ_c, the characteristic times are assumed to follow a distribution $D(\tau_c)$. This is the case in, for example, inhomogeneous samples. The total noise spectrum is then the result of all these Lorentzians, each with their own characteristic time, drawn from the distribution $D(\tau_C)$ [12]:

$$S(\omega) = \int \frac{\tau_c}{\omega^2 \tau_c^2 + 1} D(\tau_c) \mathrm{d}\tau_c. \tag{2}$$

Furthermore, the assumption is made that each of these characteristic times is thermally activated with activation energy E:

$$\tau_c = \tau_{c,0} \exp\left(E/k_B T\right), \tag{3}$$

where T is the temperature, k_B the Boltzmann constant and $\tau_{c,0}$ the inverse of the Debye frequency ν_D, which can be calculated for different interconnect materials based on their Debye temperature θ_D:

$$\tau_0 = \frac{h}{k_B \theta_D}. \tag{4}$$

Here h the Planck constant. For Cu, τ_0 is $1.4 \cdot 10^{-13}$s, for Ru $8 \cdot 10^{-14}$s and for Co $1.08 \cdot 10^{-13}$s.
The distribution of characteristic times then depends on the distribution of the activation energies, $D(E)$. The power spectral density, PSD or $S(\omega, T)$ is obtained by substituting τ_c in eq. (2) with the expression in eq. (3) and be written as [12]:

$$S(\omega, T) \propto \int f(E, \omega, T) D(E) \mathrm{d}E, \tag{5}$$

with

$$f(E, \omega, T) \equiv \frac{\tau_{c,0} \exp\left(E/k_B T\right)}{1 + \omega^2 \tau_{c,0}^2 \exp\left(2E/k_B T\right)}. \tag{6}$$

In the above equations, ω is the radial frequency and T, k_B and E are as defined before.
The maximum of $f(E, \omega, T)$ in eq. (6) is reached for:

$$\bar{E} = -k_B T \ln\left(\omega \tau_{c,0}\right). \tag{7}$$

The model of Dutta et al. tries to explain a 1/f noise spectrum (defined as $S(f) \sim 1/f^\alpha$ with $0.8 \leq \alpha \leq 1.4$)[14]. This is obtained by assuming a slowly varying $D(E)$ as compared to $k_B T$ (the width of $D(E)$ is assumed to be much larger than $k_B T$). The integral in (5) can be solved using the assumption

of a slowly varying $D(E)$ over k_BT and results in the following approximation for the power spectrum:

$$S(\omega, T) \propto \frac{k_B T}{\omega} D(\bar{E}), \tag{8}$$

which indeed corresponds to a $1/f$ noise spectrum. In the DDH-model, a distribution of activation energies $\mathrm{D}(\bar{\mathrm{E}})$ is then calculated based on the temperature dependence of the LFN PSD, evaluated at a specific frequency.

$$D(\bar{E}) \propto \frac{\omega}{k_B T} S(\omega, T). \tag{9}$$

The activation energy $\bar{E}$ or $\mathrm{E_A}$, is defined by the maximum in $D(\bar{E})$ (in what follows also denoted by $D(E_A)$) as given in eq. (7). In the application of the model, generally only eq. (7) and (9) are used. Note that to calculate $\mathrm{D(E_A)}$, the DDH-model uses 3 explicit assumptions: (1) the 1/f noise is caused by a superposition of random fluctuations with thermally activated characteristic times; (2) the distribution of activation energies $\mathrm{D(E_A)}$ must be 'smooth', that is slowly varying over k_BT; and (3) the attempt frequency $f_0 = 1/\tau_0 \gg f$, with f the frequency at which the noise is measured.

In ref. [5], we have introduced an adaptation of the DDH-model, that provides a stronger theoretical basis than the original model. Nevertheless, it was found that the original DDH-model, as presented here, is very useful for the calculation of activation energies in nanoelectronic interconnects.

In order to compare the activation energies obtained by LFN measurements, standard accelerated electromigration tests have been carried out. These are done on packaged samples using classical 4-point structures. Accelerated test conditions (current densities in the range of 1 to 5 $\mathrm{MA/cm^2}$ and temperatures between 250 and 300°C) are applied and the resistance of the line is monitored as a function of time. The failure time is defined as the moment when a 20% change in resistance occurs. From the resulting lognormal failure time distributions, the Median Time to Failure (MTF) can then be calculated and inserted in Black's law such that the activation energy can be calculated and the EM lifetime can be extrapolated to normal operation conditions.

2) Experimental results: Fig. 2 (a) shows the temperature dependence of the LFN PSD, evaluated at 5Hz, for a 30 nm wide Cu interconnect with TaNTa barrier/liner. A maximum in PSD can be observed around 65°C. Fig. 2 (b) is then obtained using eq. (7) and (9) and an activation energy of $0.76 - 0.78$ eV is found. Upon comparing this value with the activation energy obtained by standard accelerated tests (0.74 eV), they were found to be very similar. Note that the LFN activation energy was obtained without inducing damage in the metal line, contrary to the standard test method.

The LFN methodology was tested on different types of interconnects, each with different barriers, liners and/or capping materials (sample details can be found in ref. [4]). Fig. 3 shows a direct comparison of the LFN activation energy and the EM activation energy (obtained using accelerated testing and Black's law). The dashed line indicates the 1 to 1 correlation between both values. A 92% correlation between the EM and LFN $\mathrm{E_A}$ was found. This indeed provides strong evidence that LFN measurements can be used to calculate the EM activation energy in electronic interconnects.

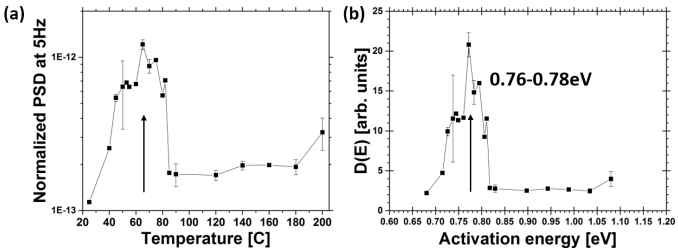

Fig. 2: (a) PSD at 5Hz as a function of temperature, measured on a 30 nm wide Cu interconnect with TaNTa barrier/liner. (b) Calculated distribution of activation energies using eq. (7) and (9). The maximum in PSD at ~ 65°C corresponds to an $\mathrm{E_A}$ of $0.76 - 0.78$eV.

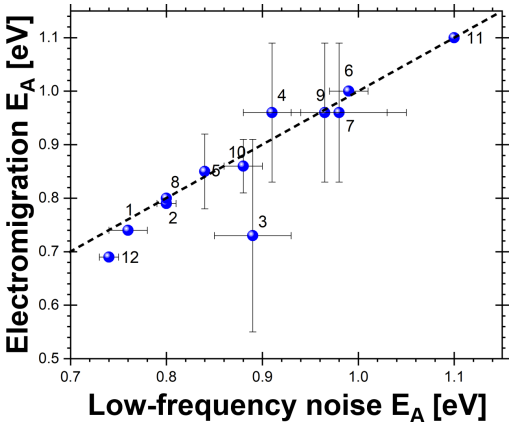

Fig. 3: Comparison of the calculated LFN $\mathrm{E_A}$ and EM $\mathrm{E_A}$ for different types of interconnects, each with different barriers, liners and/or capping materials. The dashed line indicates the 1 to 1 correlation between both values. A 92% correlation between the EM and LFN $\mathrm{E_A}$ was found.

B. Early electromigration damage detection

Low-frequency noise measurements can also be used to study early signs of electromigration damage. In ref. [4], we demonstrated that when an interconnect is subjected to EM stress, the LFN spectrum exhibits changes before a resistance increase is detected. Fig. 4 shows both the resistance and PSD (evaluated at 10Hz) as a function of stress time for a 22 nm wide Cu line with 3 nm TaN barrier and 1 nm Ru liner, subjected to EM stress (200°C and 50 $\mathrm{MA/cm^2}$). The resistance only increases after 330 min of stress, but the LFN PSD increases already when the first voids are being formed. This illustrates that low-frequency noise measurements can be used for early electromigration damage detection.

C. Qualitative electromigration lifetime prediction

Finally, it was demonstrated that LFN measurements can provide qualitative EM lifetime predictions. Because the LFN

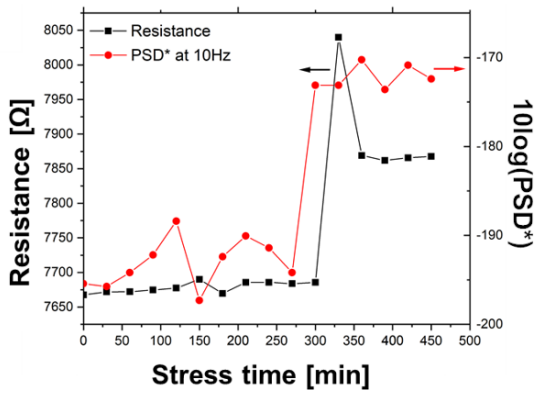

Fig. 4: Resistance and PSD (evaluated at 10Hz) as a function of stress time for a 22 nm wide Cu line with 3 nm TaN barrier and 1 nm Ru liner, subjected to electromigration stress (200°C and 50 $\mathrm{MA/cm^2}$). The LFN PSD increases prior to a noticeable change in resistance.

measurement technique is non-destructive and activation energies can be obtained on individual dies, it is possible to study die-to-die variability of EM properties. The previous section demonstrated that the LFN PSD magnitude is sensitive to defects. It was shown that this LFN PSD magnitude is roughly inversely proportional to the time to nucleate a void, as expected because void nucleation is strongly impacted by the initial defect concentration. The more defects, the shorter the void nucleation time. Furthermore, it has been shown that using both the LFN PSD magnitude and $\mathrm{E_A}$, qualitative predictions can be made regarding the time it takes to grow a void, using the following expression:

$$t_f \propto \frac{1}{A} \cdot \frac{-\log(\mathrm{PSD}^*) k_B T}{e\rho j} \exp\left(\frac{E_A}{k_B T}\right). \qquad (10)$$

The temperature, T, and the current density, J, are defined by the experimental conditions, V and Z^*e are the void volume and effective charge number times the elemental electron charge, respectively. These are expected to be constant for a given technology. A is the electrical area and ρ the electrical resistivity, which can be calculated for each sample by temperature coefficient of resistance (TCR) measurements. PSD^* is the normalized PSD at 1Hz and at a given temperature and E_A the activation energy, these parameters can be defined for each sample by means of LFN measurements. Both the nucleation and growth models were successfully verified experimentally [4, 15].

IV. Electromigration mechanisms in scaled Cu interconnects

The purpose of this section is to understand which diffusion mechanisms are driving EM failure in highly scaled Cu interconnects, that is in Cu interconnects with sub-30 nm line-widths. To do so, the LFN methodology was applied.

In ref. [24] we showed that scaling the line-width below 30 nm has a negative effect on the EM reliability of Cu interconnects. The EM activation energy was found to drop by ~ 0.05 eV as the electrical area was decreased by $400\mathrm{nm}^2$ and the lifetime was nearly halved when scaling from 32 to 22 nm line-width, with the strongest drop below 28 nm. This was attributed to an increased number of grain boundaries (confirmed by TEM analysis) and therefore enhanced grain boundary diffusion in narrow lines. Note that the initial defect concentration in these samples was high, such that defects in the vicinity of grain boundary triple points, or at grains touching the top surface, likely acted as void initiation sites.

In ref. [3] and [25], we studied the EM mechanisms in 30 nm wide lines. All of the polycrystalline Cu samples revealed an activation energy close to 0.8 eV. Comparison to the lines with columnar grains, where an activation energy of 0.8 eV is absent, reinforces the hypothesis that this value is related to grain boundary diffusion.

In ref. [26] we showed a brief comparison of the activation energies obtained in 22 nm wide Cu lines with different barriers, liners and caps. In what follows, these results are briefly revised and discussed in more detail. The sample details are shown in Table I, the color coding in Fig. 5. Details of processing and integration can be found in ref. [27]. The samples *TaNCo* and *TaNCo-Co* allow studying the effect of a 1 nm Co cap on the EM performance. The *TaNCo*, *TaNRu* and *Mn-based-Ru* samples allow benchmarking the Co vs Ru liners. The *Mn-based Ru* samples allowed investigating the Mn-silicate self-formed barrier, which is an interesting alternative for the thick TaN barrier [27, 28]. The asterisk in the last column of Table I, indicates that in one of these sample types, prior to Cu plating, an in-situ post-deposition Ru anneal was carried out (5 min in $\mathrm{H_2/Ar}$ at 350°C).

Low-frequency noise measurements were used to calculate the activation energies in the $0.7 \rightarrow 1.1$ eV range. In many cases, two activation energies were found. The results are summarized in Fig. 6, where the x-axis shows the lower $\mathrm{E_A}$ and the y-axis the higher $\mathrm{E_A}$. The upward arrow on the TaNCo + Co cap + SiC cap sample indicates that no second activation energy was detected. The error bars are due to the spread in activation energy obtained on different samples.

In what follows, each of the datapoints in Fig. 6 will be discussed.

A. *TaNCo with and without cobalt cap*

The following conclusions regarding *TaNCo* can be drawn: (1) TaNCo with and without an additional (thin) Co cap cannot effectively suppress the low activation energy ≈ 0.85 eV. An additional Co cap might increase the second activation energy to higher values, but if the dominant diffusion path is the one corresponding to 0.85 eV (which would be the case under normal operation conditions), this improvement becomes irrelevant. Thus, a thin Co cap alone will no longer be effective in deeply scaled copper interconnects.

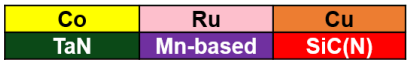

Fig. 5: Color coding used in Table I.

TABLE I: Description of the 22 nm half-pitch Cu interconnects. The color coding is shown in Fig. 5. *In one type of Mn-based Ru samples, a post-deposition Ru anneal (5 min in H_2/Ar at 350°C) was performed prior to the Cu plating.

	TaNCo	**TaNCo-Co**	**TaNRu**	**Mn-based Ru**
Barrier	3 nm TaN	3 nm TaN	3 nm TaN	1 nm Mn-based
Liner	1 nm Co	1 nm Co	1 nm Ru	1 nm Ru(*)
Cap	SiC(N)	Co + SiC(N)	SiC(N)	SiC(N)
Cross Section	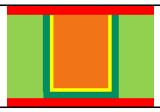	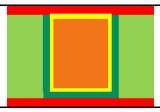		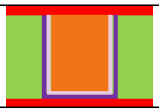

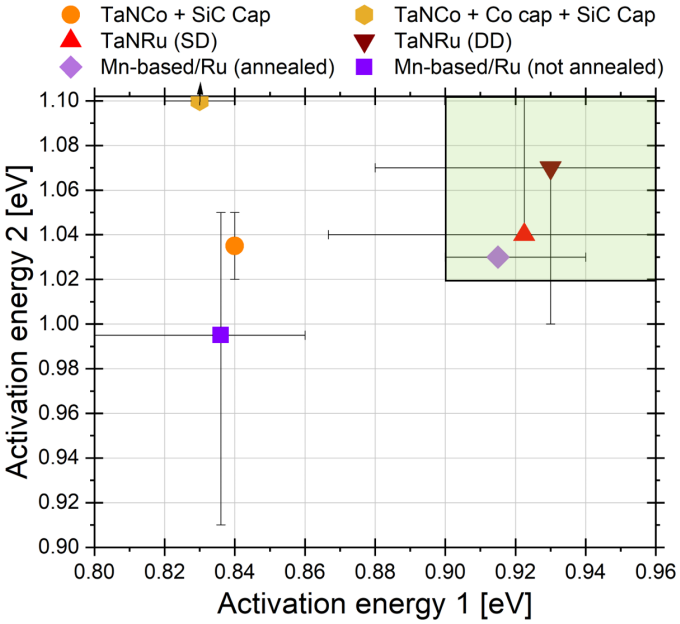

Fig. 6: Summary of the activation energies obtained by LFN measurements in the $0.7 \rightarrow 1.1$ eV range, for the different interconnect types given in Table I. The green box indicates the optimal barrier/liner stacks from an EM point of view.

(2) That the activation energy of ≈ 0.85 eV is not impacted by a (stable) Co liner in combination with at TaN barrier, indicates that in these particular samples grain boundary diffusion continues to be the dominant mechanism for EM failure. Doping defects with Co may enhance the grain boundary diffusion activation energy close to the top surface, on the condition that this interface itself remains stable.
(3) The LFN measurements revealed a thermal effect causing a decrease in activation energy and LFN PSD that may be related to mobility of Co from the cap. During processing, temperatures higher than 200°C are reached, so diffusion of Co into Cu would already have started. In this particular case, it seems that additional heating of the samples continues this process, further degrading the Co cap. The hypothesis is illustrated in Fig. 7 and premises that the Co atoms may diffuse to Cu-deficient areas such as voids or oxide, thereby reducing the interconnects' overall defectivity. This would in its turn, lead to a lower LFN magnitude. Concurrently, if Co

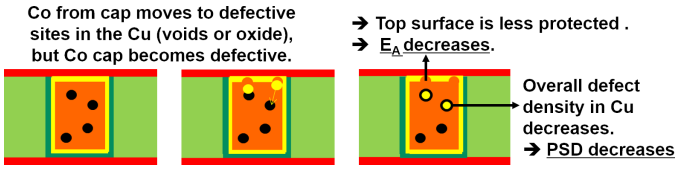

Fig. 7: Illustration of the hypothesis of mobile Co in *TaNCo-Co* samples, with Co moving from the cap to defective Cu locations. This effect reduces the overall defect density, which explains the decrease in LFN magnitude, but the Co cap may become defective such that the top surface is less protected, explaining the decrease in E_A.

is depleted from the cap, it becomes defective and no longer protects the top surface. It should be noted that the Co cap in these particular samples was indeed very thin (only ~ 1 nm). A thicker Co cap could prevent the Co cap from becoming too defective. The effect of Co-cap depletion on the grain boundaries near the surface is the following: Initially, the grain boundary activation energy would be enhanced by alleviating defects close to grain boundary triple points, but as the Co-cap degrades, grain boundaries in proximity of the defective cap will become weaker and therefore have a lower activation energy. Note that the possibility of Co, diffusing from the liner into the Cu, was not considered here because the thermal effect was not observed in the *TaNCo* samples (without Co cap).

B. TaNRu

In Fig. 6, the activation energies of both single and dual damascene *TaNRu* interconnects are shown. These barrier/liner stacks exhibited quite a large variability, but in most of the *TaNRu* interconnects, the lower E_A is increased to values > 0.9 eV. The higher E_A remains similar as for *TaNCo*, though in some samples a second E_A was not observable. The effect of a Ru liner, will become more clear in the next paragraph, where it is studied in combination with a Mn-based barrier. The reason for the enhanced EM performance is likely related to a less defective Cu/Ru interface, although a full analysis and understanding of the observation is still necessary.
It was recently shown that Cu has a much larger grain size on Ru than on Co [32]. Given the importance of grain boundary diffusion in our samples, this might explain part of the difference in activation energy between *TaNRu* and *TaNCo*.

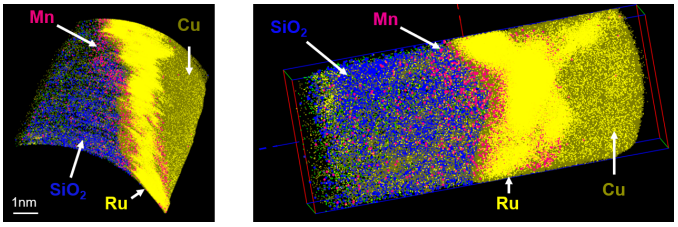

Fig. 8: APT cross sections of the sidewall of *Mn-based Ru* lines *with* anneal. The different elements are labelled in their respective color coding. The Ru liner is strongly discontinuous and found to have diffused in the Cu. The Cu composition is 99.86% with 0.14% Ru.

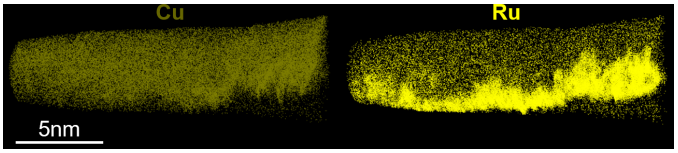

Fig. 9: APT image along the Cu/Ru interface of a *Mn-based Ru* lines *with* anneal, showing a non-uniform Ru liner and strong Ru signal in the Cu.

C. Mn-based Ru with and without post-deposition Ru anneal

For the Mn-based Ru samples *without* post deposition Ru anneal, a first activation energy ranging from $0.80 - 0.85$ eV and a second $\mathrm{E_A}$ of ≈ 1.03 eV was observed, though this higher $\mathrm{E_A}$ was not consistently visible in all of the samples. In the Mn-based Ru samples *with* post-deposition Ru anneal, an increase in lower activation energy to $0.90 - 0.94$ eV was observed. A second $\mathrm{E_A}$ of ≈ 1.03 eV was visible in only a few samples.

The activation energies of the *Mn-based Ru* lines *with* anneal, are very similar to those of the best *TaNRu* samples. This is most likely due to the Ru liner.

Fig. 8 shows two APT cross sections of the sidewall of a *Mn-based Ru* line *with* anneal. Note that a different color coding is used than in Fig. 5. The $\mathrm{SiO_2}$ dielectric, Mn-based barrier, Ru liner and Cu bulk can clearly be distinguished. The Mn-based barrier is very thin and seems to interact with $\mathrm{SiO_2}$, presumably to form a Mn-silicate. This has been discussed in detail in ref. [33]. The Ru liner is much more pronounced than the Mn-based barrier, but is strongly discontinuous. Moreover, diffusion of Ru into the Cu is observed, as well as some Cu-Ru intermixing. The Cu composition was determined to be 99.86% with 0.14% Ru.

In Fig. 9, an APT section along the line is shown. Again the Ru liner is seen to be strongly non-uniform. The distinct Ru signal originating from the Cu line, indicates diffusion of Ru from the liner into the Cu. Mn also appears on the other side of the Ru barrier, but its concentration profile could not be confirmed. Note that the post-deposition Ru anneal was performed prior to Cu plating, such that the movement of Ru into Cu cannot be occurring during this anneal. It most probably happens due to the final 20-min long BEOL anneal at $420°\mathrm{C}$.

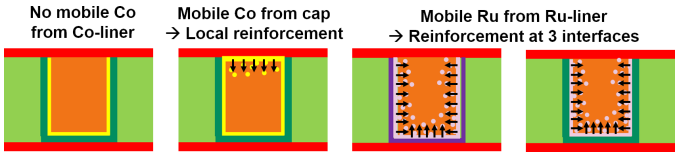

Fig. 10: Schematic illustration of how mobile Ru from a Ru liner reinforces the Cu in more locations than mobile Co originating from the Co cap.

A possible hypothesis for the improved activation energy in the samples with post-deposition Ru anneal is that it makes Ru more mobile such that it can diffuse to the Cu grain boundaries, thereby increasing the activation energy. A similar effect could be happening in the *TaNRu* lines with high EM-resistance.

The composition of the center of the line could not be analyzed because it was not possible to include it during APT sample preparation, but Fig. 9 reveals that Ru is detected up to at least 5 nm from the interface. Fig. 10 shows how this can then also explain why Ru diffusion would significantly improve the EM $\mathrm{E_A}$ and Co only marginally; evidence of mobile Co was found for a Co cap but not for a Co liner, so that leaves only one surface with reduced defectivity, as compared to three in the case of a Ru liner with mobile Ru. Of course this hypothesis is only valid for interconnects where local defects and/or grain boundaries play a dominant role. Moreover, doping of the grain boundaries is not always preferred because it increases the resistivity.

Finally we can compare our result again to the recent publication [32], where an improved EM lifetime was obtained thanks to a post-deposition Ru treatment and attributed to reduced oxygen concentration at the Ru/Cu interface. Our data does not contradict this hypothesis, on the contrary, it is a well established fact that oxygen drives diffusion of metals such as Co and Ru, leading to the intermixing with Cu that was observed in Fig. 9.

D. Summary

From Fig. 6, it can be concluded that a low $\mathrm{E_A}$ of $0.80 - 0.85$ eV is found for most of the 22 nm wide interconnects, which was previously linked to grain boundary diffusion [3, 18, 25]. Neither a Co liner, nor a Co cap, could suppress this lower activation energy. Ru liners, however, were found to increase this $\mathrm{E_A}$ to values above 0.90 eV. Mn-based barriers in combination with a Ru liner, required a post-deposition Ru anneal to obtain the same increase in activation energy. The enhanced EM performance could be explained by diffusion of Ru into Cu, as demonstrated by the APT images in Fig. 8 and 9. The use of LFN measurements greatly benefited this study, since it allowed to calculate activation energies even when standard EM tests were not possible (no flux divergence point available, tests too time consuming or only limited number of samples).

V. Electromigration in alternative metal interconnects

As the scaling of interconnect line-widths continues, Cu will eventually reach its limits as the material of choice. Below 10 nm line-width, the resistivity of Cu becomes unacceptably high and its EM performance insufficient [10, 18]. Therefore, potentially barrierless alternative metals to replace Cu are being investigated. In this section, we discuss the EM performance of 3 such candidates: ruthenium, cobalt and tungsten. Especially ruthenium proves to be of particular scientific interest because it is a p-type metal; its majority charge carriers are holes. EM failures in Ru where extensively discussed in ref. [34].
It should be noted that EM experiments on alternative metals are challenging because they require very high temperature and current density in order to observe failures within a reasonable amount of time. Therefore, LFN measurements had to be used to obtain the EM activation energy. Where possible, the LFN activation energies are compared to the results obtained using standard EM tests. It then becomes clear that at highly accelerated conditions, such as needed to characterize EM in Ru, questions may arise regarding the validity of Black's law to predict lifetimes at moderate temperatures and current densities.

A. Sample description

Five types of ruthenium, one cobalt and one tungsten interconnect have been studied, their details can be found in Table II. Four types of Ru are fabricated using the subtractive patterning technique shown in ref. [35] and one type using the spacer defined integration scheme described in ref. [36] with aspect ratio (AR) 1. We refer to these 2 types of lines as 'Metal etch' and 'Spacer-defined Ru'. The Ru lines are $7\mu\mathrm{m}$ long, other details are listed in Table II. The cobalt and tungsten lines, are fabricated using a damascene vehicle and are $100\mu\mathrm{m}$ long.

B. Results and discussion

The LFN activation energies are shown for all the samples in Fig. 11. This figure demonstrates that the $\mathrm{E_A}$ of both the Ru and Co lines is close to 1 eV. The type of process (metal etch or damascene) does not impact the Ru activation energy and neither does the difference in grain structure and surface roughness (associated with the different process conditions). In Ru, the 1 eV $\mathrm{E_A}$ is attributed to surface diffusion [37–39]. Sample $\mathrm{Ru\_3}$, does have a slightly lower $\mathrm{E_A}$ (-0.05 eV), which is attributed to its lack of adhesion layer, resulting in a weaker $\mathrm{SiO_2}$-Ru interface.
For Cobalt, the 1 eV $\mathrm{E_A}$ could be related to either grain boundary diffusion (along a polycrystalline grain structure) or the weak Co-low-k interface.
In the tungsten lines, the LFN activation energy was 0.73-0.75 eV, which is very close to the 0.69 eV found using standard EM tests [3]. This activation energy is surprisingly low for tungsten, but an analysis of its possible point defects has shown that there are several vacancy-related activation energies to be found in the 0.7 eV-range [40, 41].

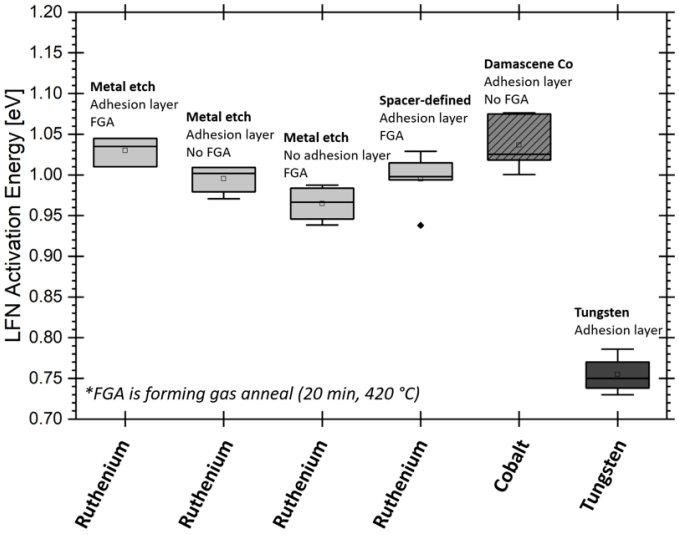

Fig. 11: Summary of the activation energies obtained with LFN measurements for the Ru, Co and W lines. The $\mathrm{E_A}$ in Ru and Co is close to 1eV; only sample type Ru_3 has a lower activation energy. A low $\mathrm{E_A}$ close to 0.7 eV is found for W (this value was confirmed using standard EM tests).

VI. Conclusions

A new EM test methodology, based on low-frequency noise measurements, was proposed and has been validated on both Cu and alternative metal interconnects by comparing the results with the ones obtained using traditional testing.
The new test method was successfully employed to study the mechanisms of electromigration in Cu interconnects. This comprises studying how the EM performance is impacted by scaling the Cu line-width and how it is affected by the choice of barrier, liner and capping materials. Finally, the LFN measurements demonstrated activation energies around 1 eV for Ru and Co and $\sim$0.7 eV for W interconnects. Using standard accelerated EM testing, the stress conditions would need to be extremely high and would be unrealistically time-consuming. The main advantages of using LFN measurements for EM characterization are that they are fast, non-destructive, provide fundamental understanding and can be done close to operation conditions.

Acknowledgment

The authors would like to thank all imec colleagues who contributed to this research, as well as the fund for scientific research in Flanders, FWO, for its funding.

References

[1] J. R. Black, "Mass transport of aluminum by momentum exchange with conducting electrons," in *Reliability Physics Symposium, 1967. Sixth Annual*. IEEE, 1967, pp. 148–159.

[2] J. Lloyd, "Black's law revisitedânucleation and growth in electromigration failure," *Microelectronics Reliability*, vol. 47, no. 9-11, pp. 1468–1472, sep 2007.

TABLE II: Sample details. FGA is Forming Gas Anneal at $420°C$ for 20min.

	Ru_1	Ru_2	Ru_3	Ru_4	Ru_5	Co	Tungsten
Process	Metal Etch	Metal Etch	Metal Etch	Metal Etch	Spacer-defined	Damascene	Damascene
Deposited Thickness	10 nm	10 nm	10 nm	8 nm	18 nm	22 nm	37 nm
Adhesion layer	0.3 nm TiN	0.3 nm TiN	NA	0.3 nm TiN	0.3 nm TiO_2	0.3 nm TiO_2	0.3 nm TiN
FGA	✓	✗	✓	✗	✓	✗	✗
Cross section $\sim nm^2$	60	60	60	35	325	1000	1600

[3] S. Beyne, K. Croes, I. De Wolf, and Z. Tőkei, "1/f noise measurements for faster evaluation of electromigration in advanced microelectronics interconnections," *Journal of Applied Physics*, vol. 119, no. 18, 2016.

[4] S. Beyne, O. Varela Pedreira, I. De Wolf, Z. Tokei, and K. Croes, "A novel electromigration characterization method based on low-frequency noise measurements," *Semiconductor Science and Technology*, vol. 34, june 2019.

[5] S. Beyne, "Electromigration mechanisms in scaled interconnects," 2019.

[6] A. Mayadas, M. Shatzkes, and J. Janak, "Electrical resistivity model for polycrystalline films: the case of specular reflection at external surfaces," *Applied Physics Letters*, vol. 14, no. 11, pp. 345–347, 1969.

[7] K. Fuchs, "The conductivity of thin metallic films according to the electron theory of metals," in *Mathematical Proceedings of the Cambridge Philosophical Society*, vol. 34, no. 1. Cambridge University Press, 1938, pp. 100–108.

[8] C.-K. Hu, R. Rosenberg, H. Rathore, D. Nguyen, and B. Agarwala, "Scaling effect on electromigration in on-chip Cu wiring," in *Proceedings of the IEEE 1999 International Interconnect Technology Conference (Cat. No.99EX247)*. IEEE, 1999, pp. 267–269.

[9] A. Oates and M. Lin, "The scaling of electromigration lifetimes," in *2012 IEEE International Reliability Physics Symposium (IRPS)*. IEEE, 2012, pp. 6B–2.

[10] K. Croes, C. Adelmann, C. Wilson, H. Zahedmanesh, O. Varela Pedreira, C. Wu, A. Leśniewska, H. Oprins, S. Beyne, I. Ciofi *et al.*, "Interconnect metals beyond copper: reliability challenges and opportunities," in *2018 IEEE International Electron Devices Meeting (IEDM)*. IEEE, 2018, pp. 5–3.

[11] P. Welch, "The use of fast fourier transform for the estimation of power spectra: a method based on time averaging over short, modified periodograms," *IEEE Transactions on audio and electroacoustics*, vol. 15, no. 2, pp. 70–73, 1967.

[12] P. Dutta, P. Dimon, and P. Horn, "Energy scales for noise processes in metals," *Physical Review Letters*, vol. 43, no. 9, p. 646, 1979.

[13] P. Dutta and P. Horn, "Low-frequency fluctuations in solids: 1 f noise," *Reviews of Modern physics*, vol. 53, no. 3, p. 497, 1981.

[14] R. F. Voss and J. Clarke, "1 f noise from systems in thermal equilibrium," *Physical Review Letters*, vol. 36, no. 1, p. 42, 1976.

[15] S. Beyne, K. Croes, I. De Wolf, and Z. Tőkei, "Direct correlation between low-frequency noise measurements and electromigration lifetimes," in *Reliability Physics Symposium (IRPS), 2017 IEEE International*. IEEE, 2017, pp. 6B–3.

[16] C.-K. Hu, L. Gignac, and R. Rosenberg, "Electromigration of Cu/low dielectric constant interconnects," *Microelectronics Reliability*, vol. 46, no. 2-4, pp. 213–231, 2006.

[17] J. Proost, T. Hirato, T. Furuhara, K. Maex, and J.-P. Celis, "Microtexture and electromigration-induced drift in electroplated damascene cu," *Journal of Applied Physics*, vol. 87, no. 6, pp. 2792–2802, 2000.

[18] A. S. Oates, "Strategies to ensure electromigration reliability of cu/low-k interconnects at 10 nm," *ECS Journal of Solid State Science and Technology*, vol. 4, no. 1, pp. N3168–N3176, nov 2014.

[19] S. Choi, C. Christiansen, L. Cao, J. Zhang, R. Filippi, T. Shen, K. B. Yeap, S. Ogden, H. Zhang, B. Fu, and P. Justison, "Effect of metal line width on electromigration of BEOL Cu interconnects," in *2018 IEEE International Reliability Physics Symposium (IRPS)*. IEEE, mar 2018, pp. 4F.4–1–4F.4–6.

[20] S. Brandstetter, V. Carreau, S. Maitrejean, M. Verdier, and M. Legros, "Grain morphology of cu damascene lines," *Microelectronic Engineering*, vol. 87, no. 3, pp. 383–386, 2010.

[21] C.-K. Hu, J. Ohm, L. M. Gignac, C. M. Breslin, S. Mittal, G. Bonilla, D. Edelstein, R. Rosenberg, S. Choi, J. J. An, A. H. Simon, M. S. Angyal, L. Clevenger, J. Maniscalco, T. Nogami, C. Penny, and B. Y. Kim, "Electromigration in Cu(Al) and Cu(Mn) damascene lines," *Journal of Applied Physics*, vol. 111, no. 9, p. 093722, may 2012.

[22] C.-K. Hu, L. G. Gignac, J. Ohm, C. M. Breslin, E. Huang, G. Bonilla, E. Liniger, R. Rosenberg, S. Choi, and A. H. Simon, "Microstructure, impurity and metal cap effects on Cu electromigration," vol. 1601, no. 1, 2014, pp. 67–78.

[23] M. H. Lin and A. S. Oates, "Electromigration in Dual-Damascene CuMn Alloy IC Interconnects," *IEEE Transactions on Device and Materials Reliability*, vol. 13, no. 1, pp. 330–332, mar 2013.

[24] S. Beyne, O. Varela Pedreira, I. De Wolf, Z. Tőkei, and K. Croes, "Low-frequency noise measurements to characterize cu-electromigration down to 44nm metal pitch," in *2019 IEEE International Reliability Physics*

Symposium (IRPS). IEEE, 2019, pp. 1–6.

[25] S. Beyne, K. Croes, I. De Wolf, and Z. Tőkei, "1/f Noise measurements for faster electromigration characterization," in *IEEE International Reliability Physics Symposium Proceedings*, 2016.

[26] S. Beyne, K. Croes, M. H. Van der Veen, O. Varela Pedreira, Q. Qi, I. D. Wolf, and Z. Tőkei, "Study of electromigration mechanisms in 22nm half- pitch Cu interconnects by 1 / f noise measurements," in *Interconnect Technology Conference (IITC), 2017 IEEE International*. IEEE, 2017, pp. 1–3.

[27] M. H. van der Veen, N. Jourdan, V. V. Gonzalez, C. Wilson, N. Heylen, O. V. Pedreira, H. Struyf, K. Croes, J. Bömmels, and Z. Tőkei, "Barrier/liner stacks for scaling the cu interconnect metallization," in *2016 IEEE International Interconnect Technology Conference/Advanced Metallization Conference (IITC/AMC)*. IEEE, 2016, pp. 28–30.

[28] J. Koike and M. Wada, "Self-forming diffusion barrier layer in Cu?Mn alloy metallization," *Applied Physics Letters*, vol. 87, no. 4, p. 041911, jul 2005.

[29] T. Standaert, G. Beique, H.-C. Chen, S.-T. Chen, B. Hamieh, J. Lee, P. McLaughlin, J. McMahon, Y. Mignot, F. Mont *et al.*, "Beol process integration for the 7 nm technology node," in *2016 IEEE International Interconnect Technology Conference/Advanced Metallization Conference (IITC/AMC)*. IEEE, 2016, pp. 2–4.

[30] T. Nogami, J. Maniscalco, A. Madan, P. Flaitz, P. DeHaven, C. Parks, L. Tai, B. S. Lawrence, R. Davis, R. Murphy *et al.*, "Cvd co and its application to cu damascene interconnections," in *2010 IEEE International Interconnect Technology Conference*. IEEE, 2010, pp. 1–3.

[31] C.-C. Yang, F. Baumann, P.-C. Wang, S. Lee, P. Ma, J. AuBuchon, and D. Edelstein, "Characterization of copper electromigration dependence on selective chemical vapor deposited cobalt capping layer thickness," *IEEE Electron Device Letters*, vol. 32, no. 4, pp. 560–562, 2011.

[32] K. Motoyama, O. van der Straten, J. Maniscalco, K. Cheng, S. deVries, C.-K. Hu, H. Huang, K. Park, Y. Kim, S. Hosadurga *et al.*, "Em enhancement of cu interconnect with ru liner for 7nm node and beyond," in *Interconnect Technology Conference (IITC), 2019 IEEE International*. IEEE, 2019, pp. 1–3.

[33] S. Beyne, L. Arnoldi, I. De Wolf, Z. Tőkei, and K. Croes, "Study of the enhanced electromigration performance of Cu(Mn) by low-frequency noise measurements and atom probe tomography," *Applied Physics Letters*, vol. 111, no. 8, 2017.

[34] S. Beyne, S. Dutta, O. Varela Pedreira, N. Bosman, C. Adelmann, I. De Wolf, Z. Tőkei, and K. Croes, "The first observation of p-type electromigration failure in full ruthenium interconnects," in *Reliability Physics Symposium (IRPS), 2018 IEEE International*. IEEE, 2018, pp. 6D–7.

[35] S. Dutta, S. Kundu, A. Gupta, G. Jamieson, J. Fernando, G. Granados, J. Bömmels, C. J. Wilson, Z. Tőkei, and C. Adelmann, "Highly Scaled Ruthenium Interconnects," *Electron Device Letters, IEEE*, vol. 38, no. 7, pp. 949–951, 2017.

[36] A. Gupta, S. Kundu, L. Teugels, J. Bommels, C. Adelmann, N. Heylen, G. Jamieson, O. Varela Pedreira, I. Ciofi, B. Chava *et al.*, "High-aspect-ratio ruthenium lines for buried power rail," in *2018 IEEE International Interconnect Technology Conference (IITC)*. IEEE, 2018, pp. 4–6.

[37] S. Beyne, O. Varela Pedreira, H. Oprins, I. De Wolf, Z. Tőkei, and K. Croes, "Electromigration activation energies in ruthenium interconnects," in *Interconnect Technology Conference (IITC), 2019 IEEE International*. IEEE, 2019, pp. 1–3.

[38] A. B. Anderson and M. K. Awad, "Binding of ru, o, and ruon (n= 1–4) to the ru (001) surface: Structures, stabilities, and diffusion barriers," *Surface Science*, vol. 183, no. 1-2, pp. 289–301, 1987.

[39] M. Chou and J. R. Chelikowsky, "Structural properties of the ru (0001) surface," *Physical Review B*, vol. 35, no. 5, p. 2124, 1987.

[40] R. Johnson, "Point-defect calculations for tungsten," *Physical Review B*, vol. 27, no. 4, p. 2014, 1983.

[41] J. Park, H. Huang, R. Siegel, and R. Balluffi, "A quantitative study of vacancy defects in quenched tungsten by combined field-ion microscopy and electrical resistometry," *Philosophical Magazine A*, vol. 48, no. 3, pp. 397–419, 1983.